A national laboratory of the U.S. Department of Energy
Office of Energy Efficiency & Renewable Energy

National Renewable Energy Laboratory

Innovation for Our Energy Future

Stress Induced Degradation Modes in CIGS Mini-Modules

Preprint

M.D. Kempe and K.M. Terwilliger
National Renewable Energy Laboratory

D. Tarrant
Shell Solar

Presented at the 33rd IEEE Photovoltaic Specialists Conference
San Diego, California
May 11–16, 2008

Conference Paper
NREL/CP-520-43302
May 2008

NREL is operated by Midwest Research Institute • Battelle Contract No. DE-AC36-99-GO10337

STRESS INDUCED DEGRADATION MODES IN CIGS MINI-MODULES

M. D. Kempe[1], K. M. Terwilliger[1], and D. Tarrant[2].
[1]National Renewable Energy Laboratory (NREL), 1617 Cole Boulevard, Golden, CO 80401
[2] Shell Solar

ABSTRACT

The stability of monolithically integrated copper (indium, gallium) (selenium, sulfur) (CIGS) based thin film solar cells on glass were evaluated as a function of highly accelerated stress testing. Mini-modules exposed to high humidity (85°C and 85% RH) had a dominant failure mechanism involving increased resistance in the ZnO:Al transparent conducting oxide. Under Dry heat (85°C and 0% RH) performance loss was much slower and involved the weakening of diodes lowering V_{oc} and loss of fill factor. These mini-modules were encapsulated using either ethylene vinyl-acetate (EVA) or a Silicone. It was found that encapsulation with EVA led to greater increases in series resistance. These experiments point to the importance of module packaging, transparent conducting oxide stability and cell integration in constructing durable CIGS modules.

INTRODUCTION

Thin film photovoltaic (PV) materials show great potential for reducing the cost of solar energy making it more broadly competitive with fossil fuels. These materials are constructed using layers only a few microns thick which greatly reduces the materials cost relative to wafer based crystalline silicon devices that are hundreds of microns thick.

CIGS based devices in particular show great promise with record small area efficiencies currently at 19.9 % [1]. However, the small distances involved with thin films also makes the possibility of diffusion of contaminants from within the layers a greater threat. Because these materials are thin films the impact of small amounts of corrosion are more likely to cause larger performance losses.

Modules are encapsulated in polymeric materials to provide mechanical support and to help protect against the corrosive influence of atmospheric moisture and other contaminants. This study was undertaken to evaluate the effects of the choice of packaging materials, laminating conditions, and moisture ingress on long term stability.

EXPERIMENTAL

Shell Solar constructed 36, 15.2 cm X 15.2 cm mini-modules from their production CIGS on glass circuit plates and contacted them using their standard methods. These modules had an active area of 172 cm^2 and consisted of 17 monolithically interconnected cells. These modules had Initial average cell parameters of: V_{oc}=0.538 V, J_{sc}=32.8 mA/cm^2, FF=65.7%, and η=11.59%.

These mini-modules were laminated using either EVA or a room temperature curing silicone (GE RTV615). Lamination with EVA was accomplished by heating the samples up to 145ºC for 8 min. Lamination with GE RTV615 included the use of Dow Corning 1200 primer to ensure good adhesion. The front-sheet was made of either glass or Tefzel™. Samples were thus encapsulated with 4 different constructions with 7 to 9 replicates each.

After encapsulation, the samples were further divided into subgroups and exposed to a stress temperature of 85ºC at either 0% RH or 85% RH for up to 8770 h. Dry conditions were obtained by running a small flow of compressed air, with a dew point of -40 ºC, through an oven held at 85 ºC. Damp heat, 85°C and 85 % RH, was obtained in a Blue M environmental chamber. Dry conditions were used to simulate the effect of perfectly functioning edge seals which are desired for production modules to pass damp heat tests.

Samples were light soaked outside in full sun for 2 hours prior to IV measurement to help minimize the effects of transient performance losses [2, 3]. IV measurements were performed on an XT-10 solar simulator using a well characterized and packaged mini-module as a reference cell for calibration. Custom software was made using Visual Basic 6.0 to assemble the IV measurements, calculate cell parameters, and organizing the results in a FileMaker Pro Database. From this the statistical software JMP IN was used to analyze the data. Changes in device parameters were calculated based on the performance after encapsulation.

IR images were taken using an Indigo Systems, Merlin™ Mid, InSb middle wavelength IR camera using the IRVista software. Images were constructed by subtracting the pixel intensity for photos taken before and after application of a current.

RESULTS

Samples exposed to 85ºC and 85% RH quickly degraded by a mechanism involving large increases in resistance in the ZnO film and some loss in open circuit voltage (V_{oc}) (see Fig.1). This drop in the V_{oc} indicates some damage to the absorber layer has taken place.

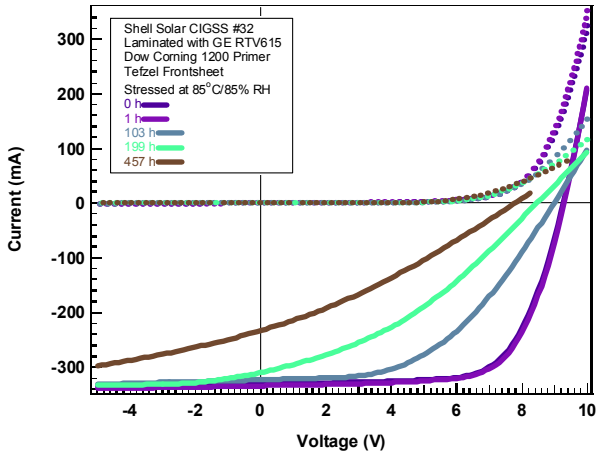

Fig. 1. IV curves of a typical module with a Tefzel front-sheet as a function of exposure 85ºC and 85% RH.

Modules laminated using an impermeable glass front-sheet had slower degradation rates than those with a Tefzel front sheet (see Fig. 2). This result was expected as EVA and silicones are known to have very high diffusivities for water [4, 6]. Over the time of this experiment one would expect moisture to penetrate the center of the mini-module package even with a glass front-sheet.

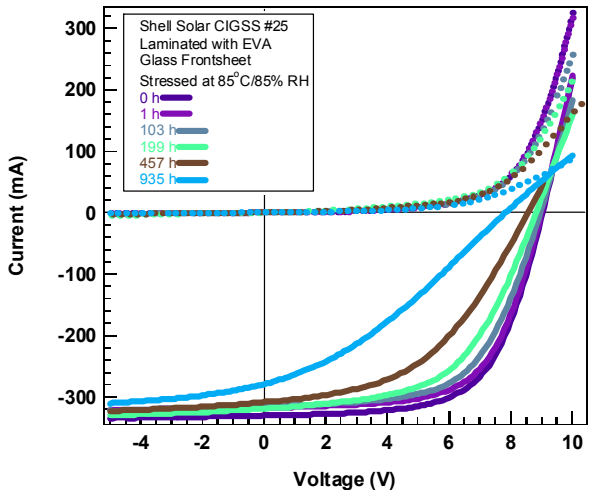

Fig. 2. IV curve of typical module with a glass front-sheet after exposure to 85ºC and 85% RH.

The change in series resistance was confirmed by infrared imaging under an applied bias (see Fig. 3). Here the heating is strongest on the side of the cell adjacent to the P1 scribe. It is not the ohmic losses in the ZnO layer that are primarily responsible for the heating. As current crosses the cell in the ZnO layer its voltage drops whereas the voltage in the Mo backcontact remains more constant because of a relatively higher conductivity. This has a net result of producing a reduction in voltage drop across the cell as one moves away from the P1 scribe. Because of the strong current voltage relationship of a diode, this small voltage drop change creates a much larger change in current causing current crowding adjacent to the scribe where current enters the ZnO layer (see Fig 4). If instead the Mo layer was much more resistive than the ZnO layer, the current crowding would be on the opposite side of the cell near the P3 scribe.

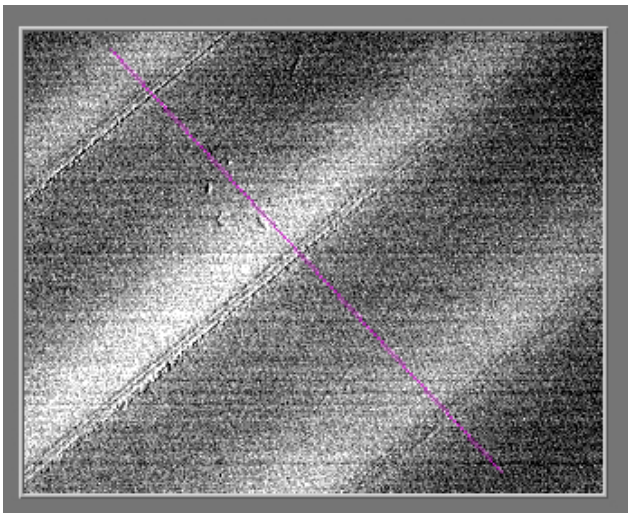

Fig. 3. Close-up infrared image of a Silicone/Tefzel encapsulated mini-module after exposure to 457 hrs of 85ºC and 85% RH. This image shows the change in temperature after the application of 81 mA at 9.5V in forward bias for 10s with no illumination.

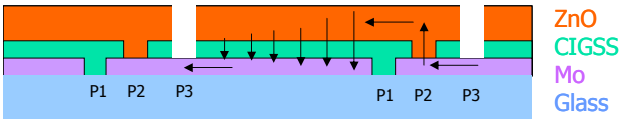

Fig. 4. Schematic of current flow through a cell with high resistance ZnO.

The effects of exposure to dry heat produced a much slower degradation allowing stress testing for a longer period of 8770 h (see Figs. 5 and 6). A two-way ANOVA (see Table 1) indicates that the choice of encapsulant affected the light series resistance (R_s, as inferred from the inverse slope at V_{oc}), the fill factor and the efficiency. Here EVA produced less desirable effects for these three factors. However, more experiments must be performed to determine if either the heat of lamination for EVA, or the use of a primer in the Silicone was a factor in this. The absence of any statistical significance in the cross terms indicates that the use of a glass front-sheet to partially trap acetic acid was not a significant factor in the degradation mechanisms.

Samples exposed to dry heat (85ºC and 0% RH) also experienced losses in V_{oc} (see Fig. 7). However, changes in J_{sc} (see Fig. 8) and light shunt resistance ($R_{sh,light}$) as

inferred by the inverse slope at J_{sc} (see Fig. 9) were statistically insignificant. Both J_{sc} and $R_{sh,light}$ changes were not shown to be dependent on the encapsulant or the front-sheet used (see Table 1). However, the module parameters *FF*, R_s, and η (see Figs. 10, 11, and 12) all showed better performance for modules laminated using a silicone rather than an EVA encapsulant.

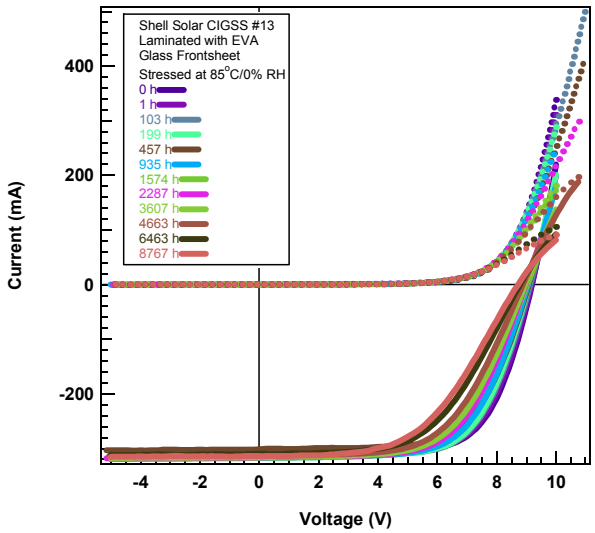

Fig. 5. Typical IV traces for a EVA/Glass encapsulated mini-module exposed to 85ºC and 0% RH.

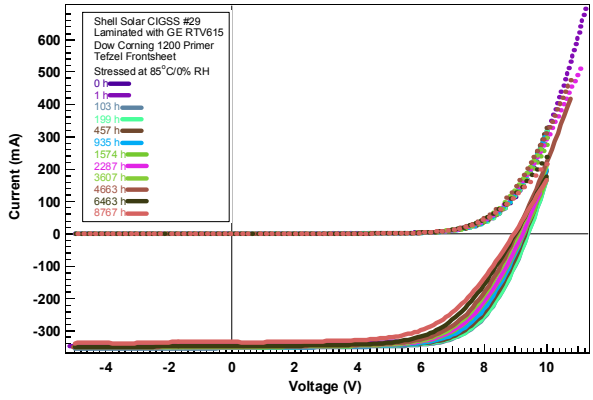

Fig. 6. Typical IV traces for a silicone/Tefzel encapsulated mini-module exposed to 85ºC and 0% RH.

Treatment		Front-sheet	Encapsulant	Encapsulant* Front-Sheet
ΔV_{oc}	F Ratio	0.005	0.55	0.14
	Probability	0.94	0.47	0.72
ΔJ_{sc}	F Ratio	0.40	0.080	1.15
	Probability	0.54	0.78	0.3
ΔFF	F Ratio	0.015	**13.5**	0.52
	Probability	0.91	**0.0036**	0.49
ΔEfficiency	F Ratio	0.16	**6.66**	0.36
	Probability	0.70	**0.026**	0.56
$\Delta R_{sh,light}$	F Ratio	1.6	0.19	0.0021
	Probability	0.23	0.67	0.96
$\Delta R_{s,light}$	F Ratio	0.0012	**8.3**	0.77
	Probability	0.97	**0.0149**	0.40
$\Delta R_{sh,dark}$	F Ratio	0.27	3.16	0.047
	Probability	0.62	*0.10*	0.83

Table 1. Results of two factor ANOVA for samples exposed to 8770 h of 85ºC and 0% RH. The "F ratio" is the ratio of the uncertainty between treatments to the sample set uncertainty. "Probability" is the chance of getting this F ratio if the two treatments were actually equivalent. i.e. a large F produces a small probability of error, indicating high confidence that the observed effects of the treatments are real. The last row, "Encapsulant*Front-sheet", indicates the probability that interactions between treatments significantly affect the results.

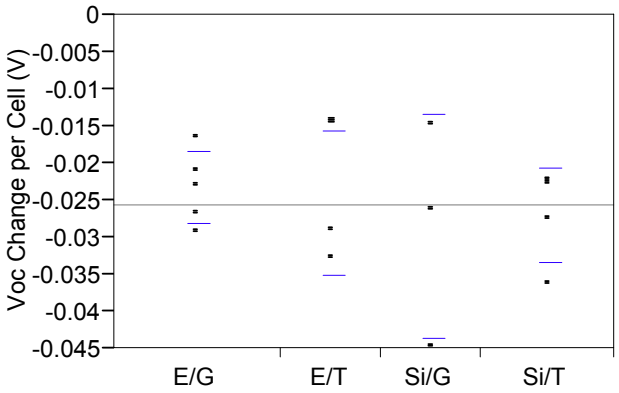

Fig. 7. Open circuit voltage change after 8770 h of 85ºC and 0% RH exposure. E=EVA, Si=Silicone, T=Tefzel, G=Glass. For this and all similar plots, the horizontal lines for each data set correspond to the 95% confidence interval for the magnitude of the changes. The large horizontal line spanning the plots is the grand mean for the data set.

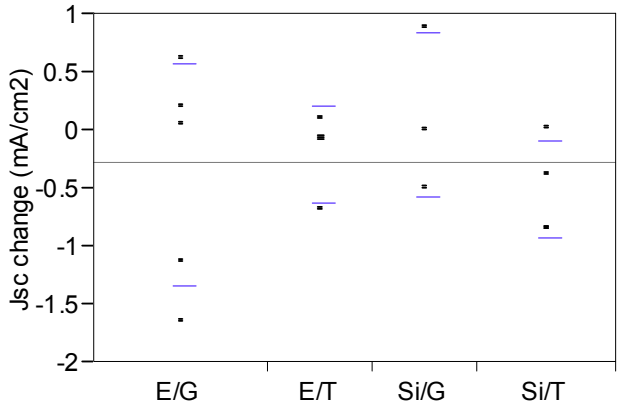

Fig. 8. Cell short circuit current change (mA/cm^2) after 8770 h of 85ºC and 0% RH exposure. E=EVA, Si=Silicone, T=Tefzel, G=Glass.

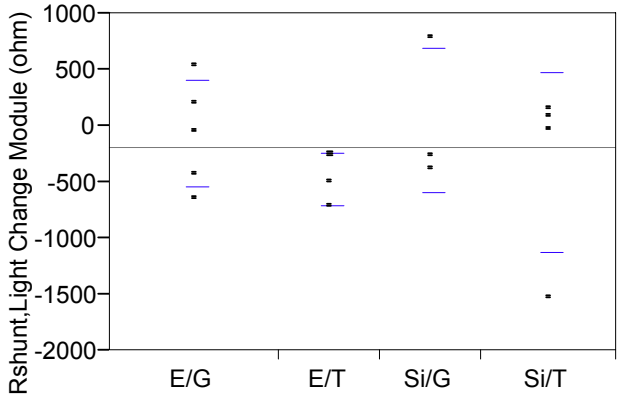

Fig. 9. Shunt resistance change (Ω) inferred from the inverse slope at J_{sc} under 1 sun illumination after 8770 h of 85ºC and 0% RH exposure. E=EVA, Si=Silicone, T=Tefzel, G=Glass.

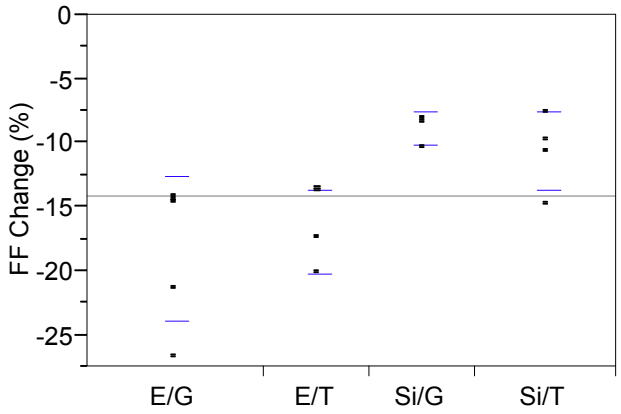

Fig. 10. Fill factor change after 8770 h of 85ºC and 0% RH exposure. E=EVA, Si=Silicone, T=Tefzel, G=Glass.

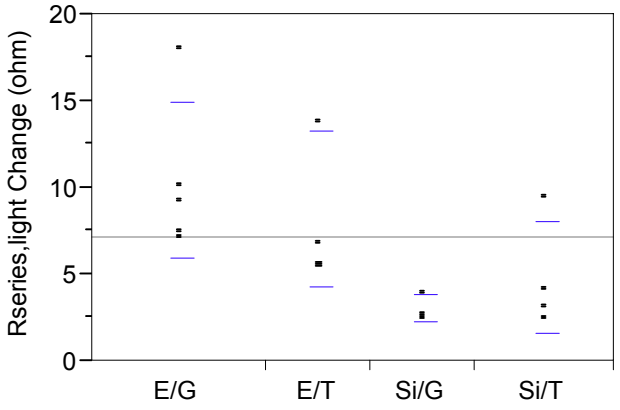

Fig. 11. Series resistance change (Ω) after 8770 h of 85ºC and 0% RH exposure. Estimated based on the inverse slope of the IV curve at V_{oc} under 1 sun illumination. E=EVA, Si=Silicone, T=Tefzel, G=Glass.

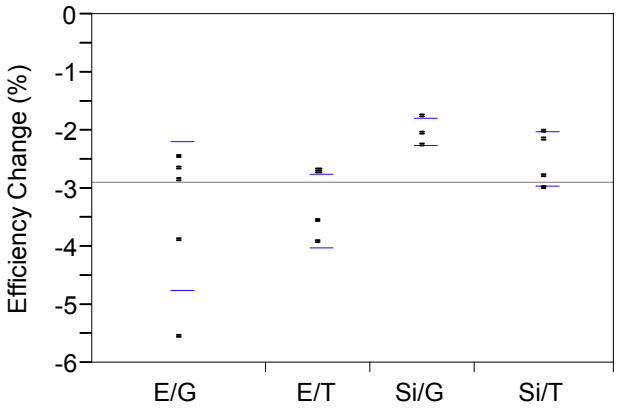

Fig. 12. Absolute efficiency change after 8770 h of 85ºC and 0% RH exposure. E=EVA, Si=Silicone, T=Tefzel, G=Glass.

At 8770 h of 85ºC and 0% RH, IR images are starting to show current crowding near the P1 scribe (see Fig. 13). This change was of a much smaller magnitude as compared to cells stressed in 85% RH (see Fig. 3) and was not easily apparent in all modules. This verifies that the change in R_s (inferred from the inverse slope of the J-V curve) is not due solely to changes in other cell properties such as the diode quality factor [5] but that it has a component attributable to ZnO resistance changes.

IR imaging was performed after application of both a forward and a reverse bias. Under forward bias hot spots can correspond to shunt paths or to weak diodes but under reverse bias only shunts show up as hot spots. Examination of IR images taken during the course of the experiment revealed more weak diodes than it did shunt paths. However, because of the lower current levels under reverse bias it is possible that this technique was less able to detect them. During stress testing, the number of weak diodes only increased slightly. There was some change in the relative intensity of the weak diodes but due to the qualitative nature of this analysis technique

we were not able to determine with confidence if specific areas were weakened.

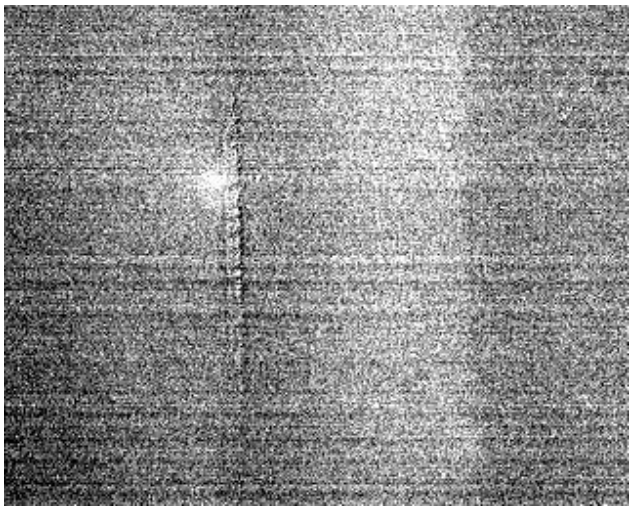

Fig. 13 Module #15 after 8770 h 85°C and 0% RH. Under forward bias of 9.5 V and 31 mA for 15 s. Constructed with EVA and a Tefzel front-sheet.

Because a Tefzel front-sheet was used in some modules, good IR radiation transmission was obtained allowing us to identify the exact location of the weak diodes (see Fig. 14). The majority of the weak diodes are located near the P1 scribe lines or along the cell edges where materials have been removed down to the glass layer (see Fig. 15). Furthermore the weak diodes located in the middle of the cells did not generally heat up as much as the other weak diodes. This indicates that the process of producing scribes and defining cells is very important for creating a CIGS module.

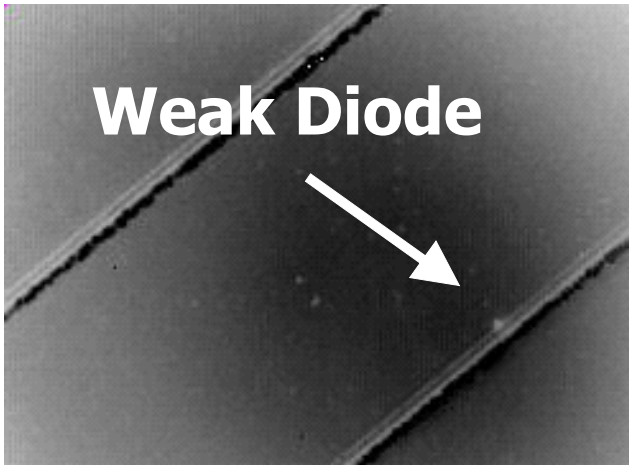

Fig. 14. IR image of a weak diode. The cell pictured was illuminated using a flashlight with the light restricted to shine only outside of the image area. This weak diode also shined brightly under forward bias.

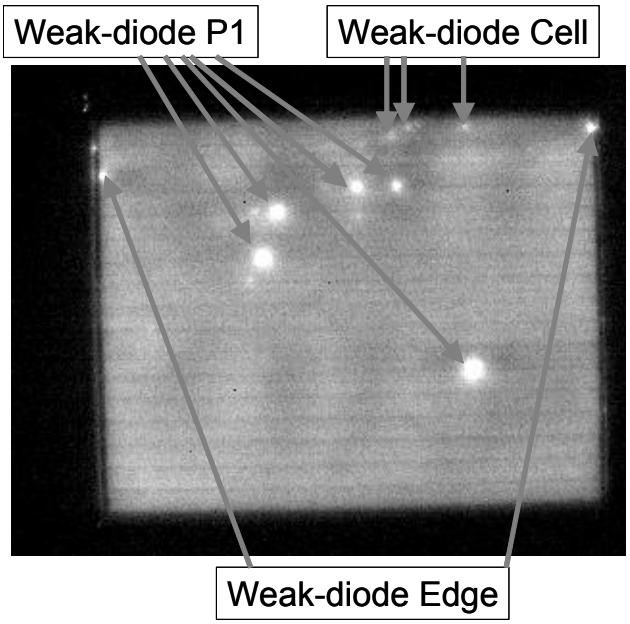

Fig. 15. IR image of a typical silicone/Tefzel encapsulated mini-module after 2290 h 80ºC and 0% RH. This image shows the change in temperature after the application of 153 mA at 9.3V in forward bias for 20s with no illumination.

Correlation coefficients were calculated comparing the variability between changes in various parameters. This yields different results than one would get if the correlation coefficients between the actual parameters was calculated. Correlation coefficients concern the deviations around the means of a sample set. With the actual parameters there would be a residual component from the onset of the experiments. Because the changes in parameters were calculated based on conditions after lamination, the correlation coefficients for the actual parameters would include information about the choice of front sheet which would affect J_{sc} in particular.

After 8770 h of dry heat, EVA samples showed a strong correlation between changes in *FF*, changes in J_{sc} and in changes in efficiency [$\text{Corr}(FF,J_{sc})_{EVA}$=0.932, $\text{Corr}(FF,\eta)_{EVA}$=0.981, and $\text{Corr}(J_{sc},\eta)_{EVA}$=0.914]. Here it should be noted that there was not a statistically significant change in J_{sc} for EVA (see Fig. 8). The presence of a strong correlation indicates that samples with a slightly improved J_{sc} had smaller changes in *FF* and conversely samples with J_{sc} losses had greater *FF* losses. This indicates a high probability that a single mechanism is responsible for most of the variability in changes in J_{sc} and changes in *FF* within the EVA sample set.

For the silicone samples, 8770 h of dry heat produced only moderately statistically significant correlations between changes in efficiency and changes in *FF* or changes in J_{sc} [$\text{Corr}(FF,\eta)_{Silicone}$=0.67, and $\text{Corr}(J_{sc},\eta)_{Silicone}$=0.64]. Furthermore, as opposed to EVA, the correlation between changes in fill factor and changes in J_{sc} with silicones were completely insignificant [$\text{Corr}(FF,J_{sc})_{Silicone}$=-0.094]. The lack of significant

correlation in silicones as opposed to strong correlation in with EVA indicates that different and/or more mechanisms are causing degradation in EVA. Because the EVA samples had both stronger correlations and greater changes in *FF* (see Fig. 10), it is probable that there exists a dominant FF degradation pathway in EVA that also affects J_{sc} but that is relatively insignificant for the silicone encapsulated cells.

The correlation between changes in *FF* and changes in series resistance losses were moderate for EVA and strong for silicone [$Corr(FF,R_s)_{EVA}$=-0.50, $Corr(FF,R_s)_{Silicone}$=-0.9434]. Furthermore, the losses related to *FF* and R_s are larger (see Figs. 10 and 11) for EVA. These facts indicate that there are a larger number of statistically significant degradation pathways leading to *FF* and R_s losses in EVA than in silicone. It is the presence multiple independent degradation mechanisms that causes this correlation to be insignificant in EVA. I.e. in Silicone one dominant degradation pathway causes both *FF* and R_s losses whereas in EVA there are two or more significant and independent pathways affecting changes in *FF* and changes in R_s.

Because EVA had such strong correlations between changes in *FF*, changes in J_{sc} and changes in efficiency, the extra degradation pathway, relative to silicones, affecting the correlation between *FF* and R_s probably only affects R_s. This may also be linked to the observation that the EVA encapsulated cells tended to have stronger inflection in the I-V curve which could also account for the larger changes in R_s inferred from the inverse slope of the I-V curve (see Figs. 5 and 6 as representative plots). Other than those mentioned here, no other strongly statistically significant correlations were found in the changes in device parameters.

The greater degradation in EVA relative to silicones may be attributable to either the higher polarity of EVA, to the production of acetic acid by-products [6], to the use of heat during lamination, or to the use of a primer with the silicone materials. More experimentation is necessary to evaluate the sources of this enhanced degradation.

CONCLUSIONS

Exposure to 85ºC and 85% RH was found to dramatically affect cells by changing the resistance of the ZnO film along with some changes to V_{oc}. Upon exposure to 8770 h of 85ºC and 0% RH, samples encapsulated using EVA experienced a statistically significant greater loss in efficiency than did samples encapsulated with silicone. EVA samples experienced greater losses in *FF* and increases in series resistance. IR images confirm that some of the changes in series resistance (inferred from the inverse slope if the IV curve) were due to changes in the ZnO resistivity rather then cell parameters such as diode quality. Changes in shunting were statistically insignificant. These loss mechanisms in dry heat result in the lowering of V_{oc} for all samples regardless of the encapsulant. IR imaging indicated only small increases in the number of weak diodes.

This study demonstrates that the method of encapsulation can affect the long term stability of CIGS modules principally through interactions with the ZnO. The effect of packaging materials on J_{sc} and V_{oc} stability was not significant. Improvements in the deposition of the ZnO or substitution with other conductors, such as indium tin oxide, may improve the stability of CIGS based devices.

ACKNOWLEDGEMENTS

The authors would like to thank Tom McMahon for helping with the infrared imaging and David Albin for help with computer code. This work was carried out under U.S. Department of Energy contract number DE-AC36-99G010337.

REFERENCES

[1] I. Repins, M. A. Contreras, B. Egaas, C. DeHart, J. Scharf, C. L. Perkins, B. To, R. Noufi, “19.9%-efficient ZnO/CdS/CuInGaSe2 solar cell with 81.2% fill factor”, *Progress in Photovoltaics: Research and Applications* **16**, 235 (2008).

[2] D. E. Tarrant and R. R. Gay, “Thin-Film Photovoltaic Partnership – CIS-Based Thin Film PV Technology”, *Final Technical Report*, NREL/SR-520-27148, October (1999).

[3]. Johnson, J. Sites, K. Ramanathan, L. Olsen, D. Tarrant, “Effects of Buffer Layers on SSI CIGSS-Absorber Transient IV and C-V Behavior”, *28th IEEE PVSC Conference*, Anchorage Alaska, (2000).

[4] M.D. Kempe, “Modeling of Rates of Moisture Ingress into Photovoltaic Modules”, *Solar Energy Materials and Solar Cells*, **90** (2006) 2720-2738.

[5] J. R. Sites, P. H. Mauk, “Diode Quality Factor Determination for Thin-Film Solar Cells”, *Solar Cells*, **27**, 411-417 (1989).

[6] M.D. Kempe, G.J. Joregensen, K.M. Terwilliger, T.J. McMahon, C.E. Kennedy, T.T. Borek, “Acetic Acid Production and Glass Transitions Concerns with Ethylene-Vinyl Acetate used in Photovoltaic Devices”, *Solar Energy Materials & Solar Cells*, **91**, 315-329 (2007).

REPORT DOCUMENTATION PAGE

Form Approved
OMB No. 0704-0188

PLEASE DO NOT RETURN YOUR FORM TO THE ABOVE ORGANIZATION.

1. REPORT DATE *(DD-MM-YYYY)*	2. REPORT TYPE	3. DATES COVERED *(From - To)*
May 2008	Conference Paper	11-16 May 2008

4. TITLE AND SUBTITLE
Stress Induced Degradation Modes in CIGS Mini-Modules: Preprint

5a. CONTRACT NUMBER
DE-AC36-99-GO10337

5b. GRANT NUMBER

5c. PROGRAM ELEMENT NUMBER

6. AUTHOR(S)
M.D. Kempe, K.M. Terwilliger, and D. Tarrant

5d. PROJECT NUMBER
NREL/CP-520-43302

5e. TASK NUMBER
PVB76701

5f. WORK UNIT NUMBER

7. PERFORMING ORGANIZATION NAME(S) AND ADDRESS(ES)
National Renewable Energy Laboratory, 1617 Cole Blvd., Golden, CO 80401-3393
Shell Solar

8. PERFORMING ORGANIZATION REPORT NUMBER
NREL/CP-520-43302

9. SPONSORING/MONITORING AGENCY NAME(S) AND ADDRESS(ES)

10. SPONSOR/MONITOR'S ACRONYM(S)
NREL

11. SPONSORING/MONITORING AGENCY REPORT NUMBER

12. DISTRIBUTION AVAILABILITY STATEMENT
National Technical Information Service
U.S. Department of Commerce
5285 Port Royal Road
Springfield, VA 22161

13. SUPPLEMENTARY NOTES

14. ABSTRACT *(Maximum 200 Words)*
The stability of monolithically integrated copper (indium, gallium) (selenium, sulfur) (CIGS) based thin film solar cells on glass were evaluated as a function of highly accelerated stress testing. Mini-modules exposed to high humidity (85°C and 85% RH) had a dominant failure mechanism involving increased resistance in the ZnO:Al transparent conducting oxide. Under Dry heat (85°C and 0% RH) performance loss was much slower and involved the weakening of diodes lowering V_{oc} and loss of fill factor. These mini-modules were encapsulated using either ethylene vinyl-acetate (EVA) or a Silicone. It was found that encapsulation with EVA led to greater losses in series resistance. These experiments point to the importance of module packaging, transparent conducting oxide stability and cell integration in constructing durable CIGS modules.

15. SUBJECT TERMS
PV; modules; monolithically integrated copper; thin film; solar cells; stress testing; transparent conducting oxide; diodes;

16. SECURITY CLASSIFICATION OF:			17. LIMITATION OF ABSTRACT	18. NUMBER OF PAGES	19a. NAME OF RESPONSIBLE PERSON
a. REPORT	b. ABSTRACT	c. THIS PAGE			19b. TELEPHONE NUMBER (*Include area code*)
Unclassified	Unclassified	Unclassified	UL		